

# Double Split-Ring Resonator Antenna Design for Optically Detected Magnetic Resonance of Nitrogen-Vacancy Centers in Diamonds

Sofia M. Davvetas<sup>1</sup>, Rashad Kadado<sup>2</sup>, Nicholas J. Curro<sup>2</sup>, and J. Sebastian Gomez-Diaz<sup>3</sup>.

<sup>1</sup>Muhlenberg College, Department of Physics, Allentown, USA

<sup>2</sup>University of California, Davis, Department of Physics and Astronomy, Davis, USA

<sup>3</sup>University of California, Davis, Department of Electrical and Computer Engineering, Davis, USA

Nitrogen-vacancy (NV) centers are spin-triplet systems with a fine structure that can be manipulated using microwave pulses. These centers can be studied through optically detected magnetic resonance (ODMR), which enables the control and detection of their spin states. To achieve this, efficient microwave pulse delivery via an antenna is crucial. This work introduces an antenna design tailored to NV centers, enabling ODMR across the relevant frequency range. The antenna is capable of operating at a single frequency or simultaneously at two frequencies. It is constructed using an FR4 board and copper. The efficiency of this antenna is demonstrated through simulations using Ansys High-Frequency Structure Simulator (HFSS).

## I. INTRODUCTION

### A. Nitrogen-Vacancy Centers

Nitrogen-vacancy (NV) centers are defects within the diamond crystal lattice that possess unique quantum properties. NV centers are particularly interesting for applications under ambient conditions. These centers form when a nitrogen atom replaces a carbon atom in the diamond lattice, with a neighboring vacancy forming adjacent to the nitrogen. NV centers

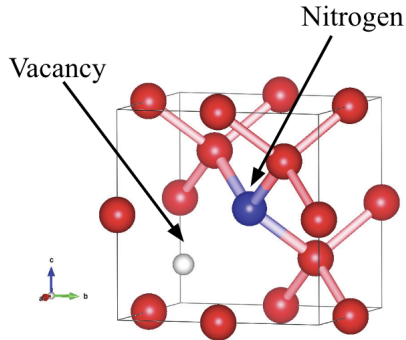


FIG. 1: NV center in diamond crystal lattice from [1].

function as spin qubits with four molecular energy levels, two of which correspond to a spin-1 system. Each spin-1 energy level has three possible spin states: 0, +1, and -1. A notable characteristic of NV centers is their zero-field splitting at approximately 2.8 GHz for the lowest triplet state,  $^3A_2$ . When a magnetic field is applied, the excited state of the NV center splits into the -1 and +1 states, for a field of 6 mT the transition frequencies for these states are at 2.7 GHz and 3 GHz, respectively. Upon transitioning from the  $^3E$  levels to the  $^3A_2$  levels, NV centers emit red light with a wavelength of 637 nm. The intensity of this fluorescence depends on the population

of spins in the spin-0 state, as spin-0 states decay through a non-fluorescent intermediate state resulting in a dip in fluorescence intensity and spin-1 states decay directly and yield stronger fluorescence than the spin-0 states.

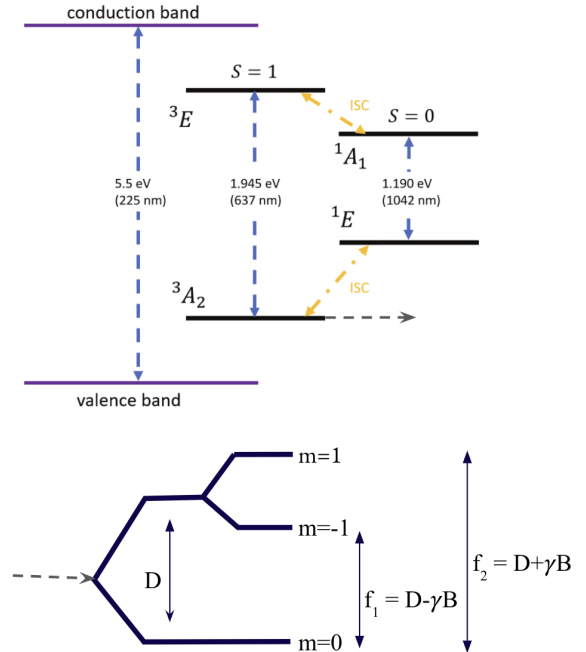


FIG. 2: Molecular energy levels for NV centers from [1] including transition frequencies.

### B. Optically Detected Magnetic Resonance

Optically detected magnetic resonance (ODMR) is a technique used to study the spin properties of materials, such as NV centers in diamonds. ODMR combines optical and microwave methods to manipulate and detect spins. In this process, the spins of NV centers can be optically polarized using

a laser with energy at least equal to that of the lowest triplet levels of the NV centers. In our setup, the ground  $S = 0$  state is optically pumped with a green laser with a wavelength of 532 nm to fully polarize the defect spin [4].

NV centers behave like atoms that are held in place and can be manipulated using microwave pulses, which drive transitions between spin states. By measuring the fluorescence intensity of the NV centers, we gain insights into the spin state, particularly the population of the spin-0 state. The fluorescence intensity is maximized when the spin is in the zero state and minimized in the +1 and -1 states. A drop in fluorescence intensity also occurs when the frequency of the microwave pulses is on resonance with the transition frequencies of the NV centers.

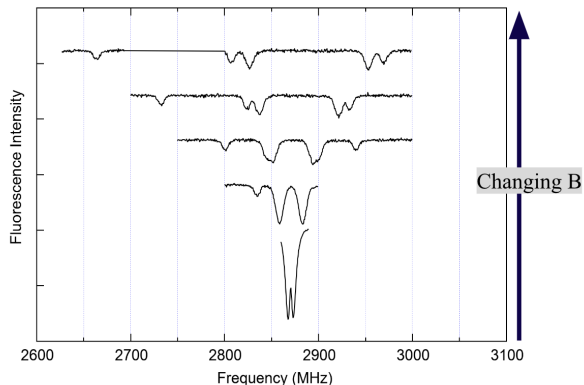


FIG. 3: On resonance fluorescence intensity dip, a magnetic field is applied to split resonance into the transition frequencies. Approximate magnetic field values from bottom to top are as follows: 0 mT, 0.3 mT, 2 mT, 4 mT, 6 mT.

### C. Rabi Oscillations

All microwave pulses in ODMR are built from Rabi oscillations. Rabi oscillations are fundamental to quantum computing and pulsed magnetic resonance, as they describe the oscillation of quantum states induced by a fluctuating magnetic field. These oscillations are triggered when a time-dependent magnetic field, such as a microwave pulse, drives transitions between different energy levels.

In our experiments, we begin by optically pumping the spins in the spin-0 state using a 532 nm laser, then we apply a microwave field at specific transition frequencies, which are near 2.8 GHz and correspond to the energy level transitions of the NV center. This microwave field initiates transitions between the spin-0 and target spin states, causing the spins to oscillate between these two states. This oscillation, known as a Rabi oscillation, occurs at a characteristic frequency called the Rabi frequency. In our setup, the Rabi frequency is 4 MHz. These Rabi oscillations can be observed for the lower transition frequency  $f_1$ , the upper transition frequency  $f_2$ , or for both simultaneously in a double quantum experiment, where

microwave pulses at both  $f_1$  and  $f_2$  are applied. The ability to control these Rabi oscillations using an antenna is critical for manipulating the quantum states of NV centers.

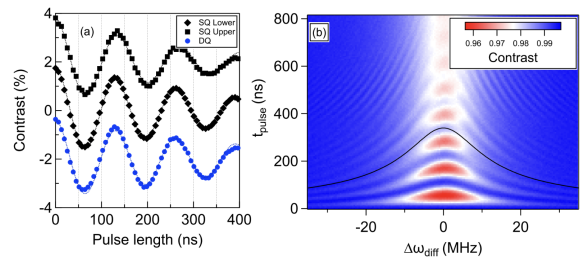


FIG. 4: (a) Rabi Oscillations fluorescence intensity. (b) Rabi oscillation fluorescence intensity for double quantum on and off resonance.

## II. CURRENT ANTENNA

### A. DC Antenna

Our current antenna is a DC antenna constructed from a glass plate with a copper loop on top, within which the diamond sample is placed. This antenna is equipped with a single port that is accessible through an SMA connector. The magnetic field and current generated by this antenna are very small; the magnetic field averaged over the area where the diamond sample is placed, is only 17 A/m. Despite these lim-

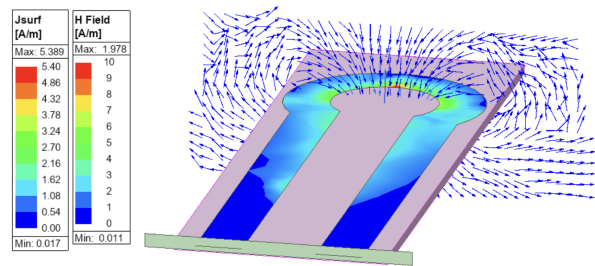


FIG. 5: DC Antenna current and magnetic field profile.

itations, we can still conduct experiments by using longer microwave pulse lengths. However, the pulse lengths required with this antenna are very long, which is problematic because we want to be able to apply shorter, more efficient pulses. NV centers have a decoherence time of only 2  $\mu$ s, giving us a very limited time frame for operations. To effectively communicate with the NV centers, we need to input a significant amount of power into the antenna, but much of this power is not reaching the NV centers, making our current antenna inefficient.

Given the substantial power input, it is likely that the power is radiating out of the cable junction. We analyze this power loss by examining the S-parameter plots.

## B. S-Parameters

To evaluate our antenna designs, we use scattering parameters (S-parameters). S-parameters provide a way to analyze a system by examining the input, reflected, and transmitted voltages. These parameters are organized into a matrix, where each element represents the ratio of output power to input power along a specific path within the system. For instance,  $S_{11}$  represents the reflected power that enters and exits through port 1, while  $S_{21}$  represents the transmitted power that enters at port 1 and exits at port 2.

By examining S-parameter plots, we can identify the resonant frequencies of our antennas, which are indicated by peaks in the plots. A strong resonance is typically characterized by a peak that dips to at least -12 dB, indicating effective energy transfer at that frequency.

Since our current DC antenna has only one port, we are only concerned with the reflected power. This antenna has a resonant frequency just below 10 GHz, which is significantly higher than the transition frequencies of NV centers. When we examine the  $S_{11}$  parameter at the relevant transition frequencies, around 2.7 GHz and 3 GHz, it measures at 0 dB. This indicates that all the power is being reflected, with none being transmitted to the NV centers.

To effectively interact with the NV centers, we need a deep resonance at their transition frequencies. To achieve this, we develop a new antenna that is specifically tuned to match the transition frequencies of NV centers in diamonds.

## III. ANTENNA DESIGN

The new antenna design incorporates two primary components: a coplanar waveguide and split-ring resonators. By utilizing the coplanar waveguide to excite the resonators, we can engineer the antenna to exhibit specific resonant frequencies that match the resonances of NV centers.

### A. Split-Ring Resonators

Split-ring resonators (SRRs) are ring-shaped structures designed to exhibit magnetic resonances. Typically fabricated from metallic materials such as copper, SRRs consist of two concentric rings with gaps aligned  $180^\circ$  apart. In our designs, the SRRs are constructed from copper. The resonant frequency of SRRs is influenced by several geometric parameters shown in FIG. 7, including the radius of the rings ( $r_1$  and  $r_2$ ), the width of the rings ( $w$ ), the width of the gaps ( $d_0$ ), and the separation between the two rings ( $d_1$ ). For design simplicity, the width and gap of the rings is kept the same for both rings. At resonance, these structures support circulating currents within the rings, resulting in a magnetic response characterized by negative permeability. The magnetic field generated by SRRs resembles the field of a magnetic dipole, as depicted in FIG. 8 (b), with a strong field component directed through the center of the SRR. Split-ring resonators (SRRs) can be effectively modeled as an RLC circuit, which includes

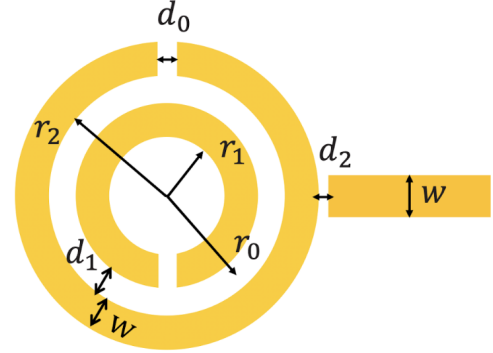


FIG. 6: Split ring resonator geometry from [2].

resistive, inductive, and capacitive components. The resistive component is due to the metallic material of the SRR, typically copper. The inductive component is created by the loop of the rings; as current flows through the loop, it generates a magnetic field, creating an inductance. The capacitive component is due to the gap in the rings where charges will accumulate on either side of the gap, effectively serving as a capacitor. The capacitance of the SRRs is influenced by the gap size, the dimensions of the rings, and the permittivity of the material between the rings. A smaller gap size results in higher capacitance. For excitation, SRRs require a transmission line; in our new antenna design, we utilize a coplanar waveguide to achieve this.

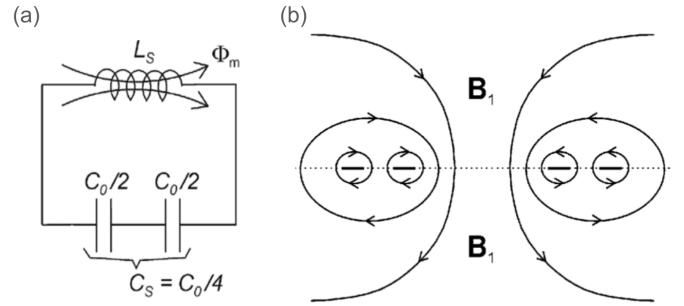


FIG. 7: (a) Split ring resonator circuit equivalent from [3] (b) SRR magnetic field profile from [3].

### B. Coplanar Waveguide

A coplanar waveguide (CPW) is an electrical transmission line designed for the transmission of microwave frequency signals. It consists of a central conductor trace positioned between two ground planes, all situated on a dielectric substrate. In our new antenna design, the dielectric substrate is

FR4 board, which has a dielectric constant ranging from 3.8 to 4.8. The effective permittivity and impedance of the CPW are influenced by several factors, including the dielectric constant of the substrate, the width of the conductor trace, the spacing between the ground planes, and the thickness of the substrate. When designing a coplanar waveguide, it is essen-

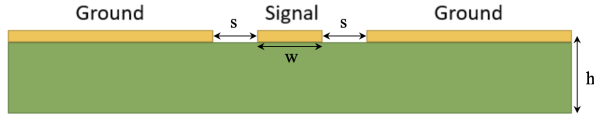


FIG. 8: Coplanar waveguide geometry.

tial to ensure that the impedance is  $50 \Omega$ . This is achieved by carefully adjusting the geometry of the CPW. In HFSS simulations, we excite the CPW using two wave ports. To verify that the waveguide is operating properly, we analyze the S-parameter plots by focusing on the transmitted power. For an ideal waveguide, there should be no power loss between the two ports. The  $S_{21}$  and  $S_{12}$  parameters should measure close to 0 dB across a broad frequency range, indicating perfect transmission and zero reflection.

### C. Antenna Geometry

Coupling the split ring resonator to the coplanar waveguide by placing it on the side of the CPW opposite to the conductor allows us to excite the SRR using the CPW. With this design, we can create an antenna with a resonant frequency of our choosing. The geometry of our antenna is optimized using of parametric sweeps. By systematically varying the parameters of the antenna, we analyze the corresponding S-parameter plots to refine its design. Specifically, we perform sweeps on

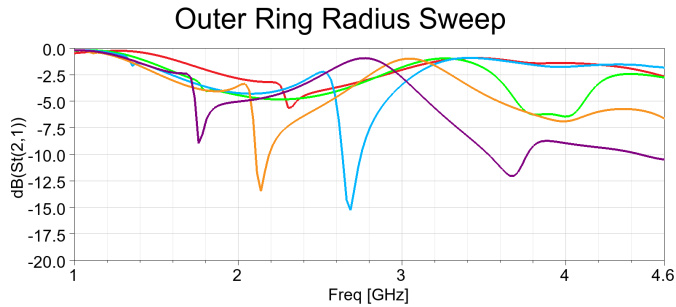


FIG. 9: Outer ring radius parametric sweep from 4 mm to 7 mm in steps of 1 mm with constant parameters  $w = 1.4mm$ ,  $d_0 = 0.4mm$ ,  $d_1 = 0.6mm$  and  $r_1$  is adjusted based on the outer radius,  $r_1 = r_2 - d_1 - w$ . The green line corresponds to  $r_2 = 4mm$ , the blue line corresponds to  $r_2 = 5mm$ , the orange line corresponds to  $r_2 = 6mm$ , and the purple line corresponds to  $r_2 = 7mm$

parameters such as the outer ring radius of the SRR, the width

of the rings, and the gap between the rings. Our analysis reveals that increasing the outer ring radius leads to a decrease in the resonant frequency. Through these parametric sweeps, we are able to hone in on separate antenna designs with resonant frequencies that match the transition frequencies of NV centers.

Altering the geometry of the split-ring resonator primarily affects the resonant frequency of the antenna but has minimal impact on the amplitude of the resonance peak. To achieve a strong resonance, where the peak depth is at least -12 dB, we adjust the dimensions of the coplanar waveguide, focusing on the substrate thickness. Reducing the thickness of the FR4 board enhances the magnetic field strength generated by the resonator, leading to a deeper resonance peak. As the substrate thickness decreases, we also modify the geometry of the CPW to maintain its characteristic impedance of  $50 \Omega$ . Our design focuses on the fundamental mode of excitation, which is represented by the first peak in the S-parameter plots. After adjustments to both the SRR and CPW, we observe pronounced resonance dips at our desired frequencies.

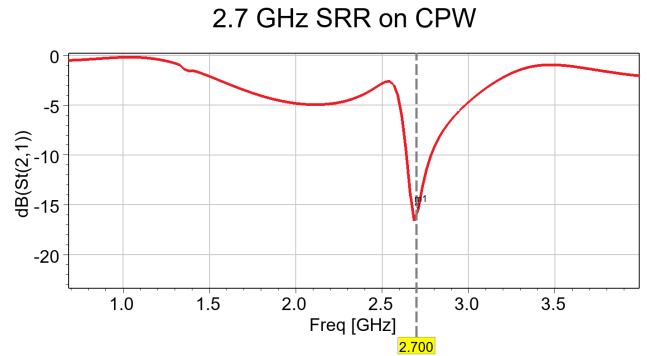


FIG. 10: Single SRR antenna transmitted power for an antenna tuned to 2.7 GHz.

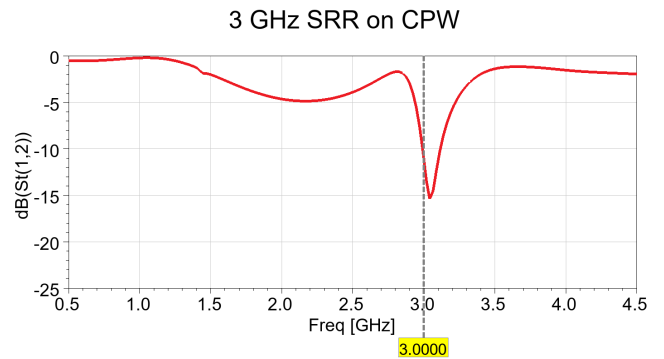


FIG. 11: Single SRR antenna transmitted power for a separate antenna tuned to 3 GHz.

## IV. RESULTS AND DISCUSSION

### A. Single Split Ring Resonator Antenna

The current and magnetic field distributions created by the antenna can be simulated using HFSS. For the antenna design with a resonant frequency of 2.7 GHz, we generate plots of the current distribution on the split-ring resonator and the magnetic field in a plane intersecting the center of the SRR.

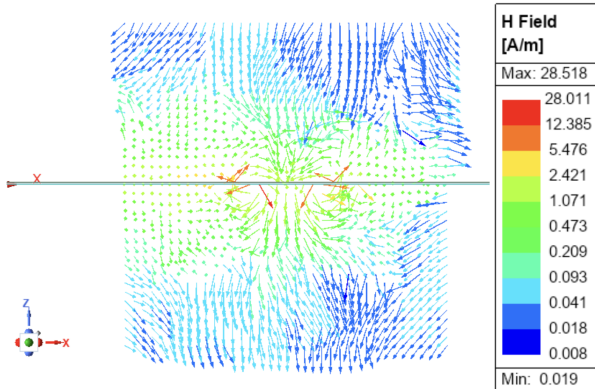


FIG. 12: Single SRR antenna magnetic field profile at 2.7 GHz, for an antenna tuned to this frequency.

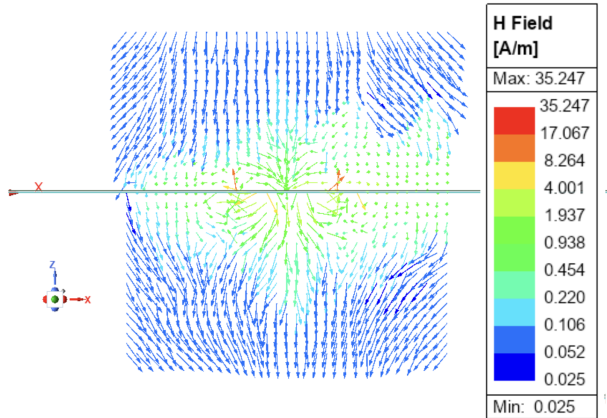


FIG. 13: Single SRR antenna magnetic field profile at 3 GHz for a separate antenna tuned to this frequency.

The magnetic field exhibits a dipole-like behavior, consistent with our expectations, reaching a maximum value of approximately 28 A/m. We perform the same simulations for the antenna design with a resonant frequency of 3 GHz, observing similar current and magnetic field profiles, with the magnetic field reaching a maximum value of around 35 A/m. Note that in this work, single split ring resonator antennas are only being tuned to one frequency, thus two of these antennas was

designed, one tuned to 2.7 GHz and a second antenna tuned to 3 GHz.

When looking at NV centers, we want an antenna that couples to both transition frequencies, rather than employing separate antennas for each frequency. Split-ring resonators are capable of supporting multiple resonant frequencies, with the separation between these frequencies being influenced by the size of the gap in the rings. For NV centers, the separation between the two transition frequencies is 0.3 GHz, which is relatively narrow and challenging to achieve with a single resonator.

### B. Double Split Ring Resonator Antenna

To achieve the small frequency separation required for NV centers, we position two split-ring resonators next to each other on a coplanar waveguide, with each resonator tuned to one of the transition frequencies. Placing the resonators in close proximity allows them to maintain strong current distributions at their respective resonant frequencies. The interaction between the two resonators gives rise to two distinct modes: in-phase and out-of-phase. These modes can be conceptualized as two oscillating swings connected by springs, where the coupling between the inductive components of the SRRs determines the characteristics of these oscillatory modes. To optimize the size of the resonance peaks

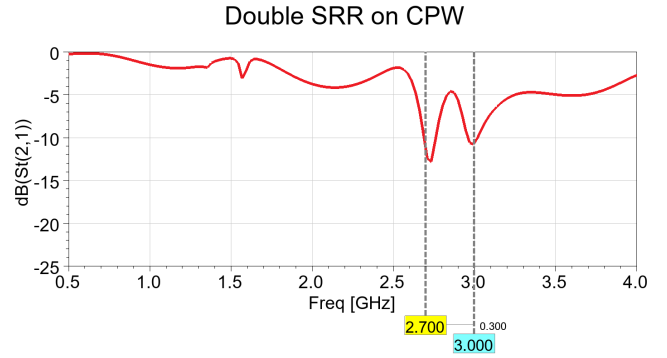


FIG. 14: Double SRR antenna transmitted power.

and their frequency values, small adjustments to the outer radius of each split-ring resonator and the separation between the two resonators were made. In the final design, the resonant peaks are observed at 2.7 GHz and 3 GHz, with magnitudes just above 12 dB, meeting the requirement for strong resonant frequencies. When examining the field distribution for the double SRR antenna at these frequencies, we note that the field patterns differ slightly between the two frequencies.

At the lower frequency, the SRRs oscillate in phase with each other, while at the higher frequency, they oscillate out of phase. This phase difference is evident when comparing the direction of the magnetic field within the SRRs. Specifically, the direction of the magnetic field at the center of the resonators reveals strong field regions oriented either upward or downward at both frequencies.

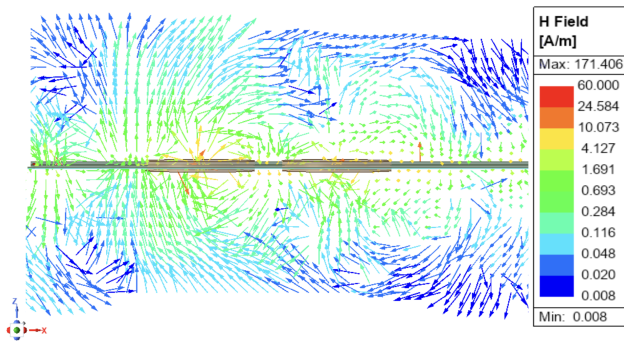


FIG. 15: Double SRR antenna H field profile at 2.7 GHz and (b) 3 GHz.

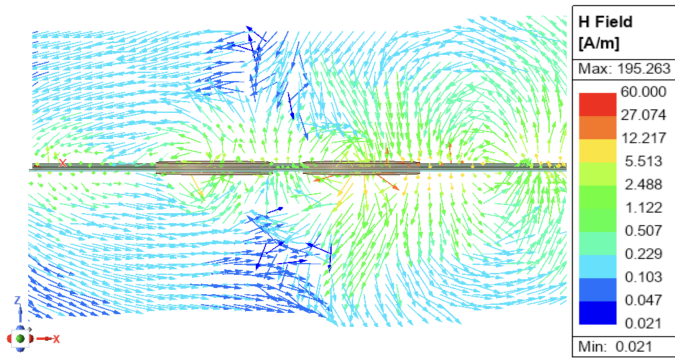


FIG. 16: Double SRR antenna H field profile at 3 GHz.

Identifying regions of strong magnetic field is crucial for determining the placement of our sample on the antenna. The sample will be positioned on the same side of the antenna as the split-ring resonators. For the new antenna design, the magnetic field averaged over the area of our diamond sample measures approximately 28 A/m. This represents an improvement compared to our current antenna, which only provides a field strength of 17 A/m. If we consider a scenario with zero losses, the magnetic field strength could theoretically be even higher, potentially reaching values above 28 A/m depending on the design efficiency and materials used.

## V. CONCLUSIONS AND FUTURE WORK

In this work, we have developed an antenna design tailored to the specific requirements of NV centers, focusing on achieving strong resonance at the target transition frequencies of 2.7 GHz and 3 GHz. Through precise adjustments to the split-ring resonator (SRR) geometry and the coplanar waveguide (CPW) configuration, we optimized the resonance peaks and magnetic field distribution. The new antenna design significantly enhances the magnetic field strength across the diamond sample, improving the efficiency of NV center manipulation.

Future work will involve fabricating and experimentally validating the antenna design. We will also adjust the design to accommodate resonances for other crystals, broadening the potential applications of the antenna. The design will be sent to PCBWay for fabrication, after which we will proceed with testing and further optimization.

- 
- [1] Casey, William H and Wang, Zhipan and Brandt, Nicholas and Curro, Nicholas, "The promise of optical nmr spectroscopy for experimental aqueous geochemistry," *American Journal of Science* **320**, (2020).
- [2] Yang, Yan and Wu, Qin and Wang, YangPeng and Chen, WuHui and Yu, Zhifei and Yang, Xiaofan and Fan, Jing-Wei and Chen, Bing, "Tunable double split-ring resonator for quantum sensing using nitrogen-vacancy centers in diamond," *Optics Continuum* **2**, 1426 (2023).
- [3] Baena, Juan Domingo and Bonache, Jordi and Martín, Ferran and Sillero, R Marqués and Falcone, Francisco and Lopetegi, Txema and Laso, Miguel AG and Garcia-Garcia, Joan and Gil, Ignacio and Portillo, M Flores and others, "Equivalent-circuit models for split-ring resonators and complementary split-ring resonators," *Optics Express* **13**, 1451 (2005).
- [4] Zhipan Wang, Christopher McPherson, Rashad Kadado, William H. Casey, Nicholas Curro, "Chapter Eight - Optically detected NMR in a diamond-anvil cell for geochemistry," *Advances in Inorganic Chemistry*, Vol. 78, pp. 269-287, 2021.